

# Where Have All the Sulfur Atoms Gone? Polycyclic Aromatic Hydrocarbon as a Possible Sink for the Missing Sulfur in the Interstellar Medium. I. The C–S Band Strengths

DRAFT: 2024.8.12.16

X.J. Yang<sup>1,2</sup>, Lijun Hua<sup>1</sup>, and Aigen Li<sup>2</sup>

## ABSTRACT

Despite its biogenic and astrochemical importance, sulfur (S), the 10th most abundant element in the interstellar medium (ISM) with a total abundance of  $S/H \approx 2.2 \times 10^{-5}$ , largely remains undetected in molecular clouds. Even in the diffuse ISM where S was previously often believed to be fully in the gas phase, in recent years observational evidence has suggested that S may also be appreciably depleted from the gas. What might be the dominant S reservoir in the ISM remains unknown. Solid sulfides like MgS, FeS and SiS<sub>2</sub> are excluded as a major S reservoir due to the undetection of their expected infrared spectral bands in the ISM. In this work, we explore the potential role of sulfurated polycyclic aromatic hydrocarbon (PAH) molecules—PAHs with sulfur heterocycles (PASHs)—as a sink for the missing S. Utilizing density function theory, we compute the vibrational spectra of 18 representative PASH molecules. It is found that these molecules exhibit a prominent, C–S stretching band at  $\sim 10 \mu\text{m}$  and two relatively weak, C–S deformation bands at 15 and 25  $\mu\text{m}$  that are not mixed with the nominal PAH bands at 6.2, 7.7, 8.6, 11.3 and 12.7  $\mu\text{m}$ . If several parts per million of S (relative to H) are locked up in PAHs, the 10  $\mu\text{m}$  C–S band would be detectable by *Spitzer* and JWST. To quantitatively explore the amount of S/H depleted in PASHs, detailed comparison of the infrared *emission* spectra of PASHs with the *Spitzer* and JWST observations is needed.

*Subject headings:* dust, extinction — ISM: lines and bands — ISM: molecules

---

<sup>1</sup>Hunan Key Laboratory for Stellar and Interstellar Physics and School of Physics and Optoelectronics, Xiangtan University, Hunan 411105, China xjyang@xtu.edu.cn

<sup>2</sup>Department of Physics and Astronomy, University of Missouri, Columbia, MO 65211, USA; lia@missouri.edu

## 1. Introduction

Sulfur (S) is the 10th most abundant element in the interstellar medium (ISM). As a biogenic element, S plays a crucial role in the biological systems on Earth (Krijt et al. 2023 and references therein). In the diffuse ISM where there are plenty of ultraviolet (UV) photons with energies exceeding 10.36 eV, the ionization potential energy of S, the predominant form of gas-phase S in the diffuse ISM is sulfur ion ( $S^+$ ). In molecular clouds, S is found in gas molecules and ices (e.g., see Mifsud et al. 2021, Hily-Blant et al. 2022, McClure et al. 2023). The abundance of S relative to hydrogen (H), S/H, is an essential parameter for understanding the interstellar gas chemistry. S-bearing molecules are often used as tracers of their kinematics and chemical evolution in star- and planet-forming clouds (Zhou et al. 1993; Wakelam et al. 2004; Dutrey et al. 1997; Le Gal et al. 2019). However, our understanding of the interstellar S/H abundance is still poor or at least incomplete: it remains notoriously mysterious regarding the possible carriers of the S elements missing from the gas phase in molecular clouds; it remains unknown whether S in the diffuse ISM is partly depleted from the gas and locked up in dust; even more fundamentally, it is not definitely clear what the true interstellar S/H abundance is.

### 1.1. What is the interstellar S/H abundance?

Elements in the ISM exist in the form of gas or dust. The interstellar gas-phase abundance of an element can be measured from its optical and UV absorption lines. The elements “missing” from the gas phase are bound up in dust grains, known as “interstellar depletion”. The total interstellar abundance of an element is the sum of its gas-phase abundance and the interstellar depletion. The interstellar depletion of an element is commonly derived from the interstellar extinction and infrared (IR) emission modeling and/or the UV (e.g., the 2175 Å extinction bump) or IR spectral bands (e.g., the 9.7  $\mu\text{m}$  silicate absorption band). This requires an assumption of dust size and composition which are often not accurately known.

Therefore, instead of summing up the gas-phase abundance and the interstellar depletion, one often assumes a “reference standard” for the interstellar abundance. Historically, the Sun is such a common reference standard, i.e., the interstellar abundances of elements are assumed to be those of solar measured from the solar photosphere. In this case, the interstellar S/H abundance would be  $[S/H]_{\text{ISM}} = [S/H]_{\odot} \approx 14.5 \pm 1.0$  ppm (Asplund et al. 2009). Because of their young ages, it had also been suggested that B stars and young F, G stars might better represent the interstellar abundances. While the carbon abundance (C/H) of B and young F, G stars are appreciably lower than solar, their S/H abundance of  $\sim 16.2 \pm 1.3$  ppm is similar to solar (within uncertainties) or somewhat higher than solar (see

Przybilla et al. 2008). Lodders (2003) pointed out that the present-day solar photospheric abundances (as well as that of B stars and young F, G stars) could be lower than those of the proto-Sun because heavy elements might have settled toward the Sun’s interior since the time of its formation  $\sim 4.55$  Gyr ago. Taking the settling effects into account, Lodders (2003) derived a protosolar S/H abundance of  $18.2 \pm 1.7$  ppm. Compared to the ISM out of which the Sun was formed 4.55 Gyr ago, the present-day ISM has been chemically enriched over the past 4.55 Gyr due to the Galactic chemical evolution (GCE). Assuming a GCE enrichment of 0.09 dex (Chiappini et al. 2003), we obtain a *recommended*, present-day interstellar S/H abundance of  $22.4 \pm 1.7$  ppm.

## 1.2. Is S Depleted in the Diffuse ISM?

In the diffuse ISM, it was once believed that S is entirely volatile and there is no S depletion in solids. However, Howk et al. (2006) measured the gas-phase S/H abundance for the Galactic halo and derived  $[\text{S}/\text{H}]_{\text{gas}} \approx 13.5$  ppm. While close to the solar abundance of  $[\text{S}/\text{H}]_{\odot} \approx 14.5$  ppm (Asplund et al. 2009), the Galactic halo gas-phase S/H abundance is considerably lower than the interstellar abundance of  $[\text{S}/\text{H}]_{\text{ISM}} = 22.4$  ppm as discussed in §1.1, implying that S is partly depleted in dust even in the Galactic halo. Howk et al. (2006) also measured the Galactic halo gas-phase abundance of iron (Fe) to be  $[\text{Fe}/\text{H}]_{\text{gas}} \approx 5.4$  ppm. Although in the Galactic halo Fe is not as heavily depleted as in the diffuse ISM, the Galactic halo gas-phase Fe/H abundance is still substantially lower than the interstellar Fe/H abundance of  $\sim 48$  ppm (see Zuo et al. 2021), indicating a significant incorporation of Fe into dust. This demonstrates that dust grains are present and survive in the hostile halo environment. Therefore, it is not unreasonable to have some portions of the interstellar S elements to be locked up in dust in the Galactic halo.

White & Sofia (2011) analyzed the strong S II 1250, 1253, 1259 Å absorption bands toward 28 interstellar lines of sight obtained with the high-resolution Space Telescope Imaging Spectrograph (STIS) instrument on board the Hubble Space Telescope (HST). Their results were consistent with the depletion of S into dust grains, although it does not follow the pattern of other elements in dust. Jenkins (2009) proposed a unified presentation of elemental depletion in the ISM and also concluded that S is depleted from the gas phase in the diffuse ISM. Hensley & Draine (2021) adopted  $[\text{S}/\text{H}]_{\text{gas}} \approx 9.6$  ppm and this would suggest a depletion of  $[\text{S}/\text{H}]_{\text{dust}} \approx 12.8$  ppm for the diffuse ISM, if we adopt an interstellar abundance of  $[\text{S}/\text{H}]_{\text{ISM}} = 22.4$  ppm.

### 1.3. Extreme Depletion of S in Dense Clouds

The S/H abundance in the dense ISM is a long-standing problem in astrochemistry (e.g., see Laas & Caselli 2019 and references therein). Many observations have shown that S depletion is far more severe in dense clouds than in the diffuse ISM. The observed abundances of S-bearing molecules in molecular clouds (e.g., CS, H<sub>2</sub>S, SO, SO<sub>2</sub> and OCS) make up a very small fraction of the S nuclei (Prasad & Huntress 1982; Anderson et al. 2013). For example, in cold dark clouds and dense cores shielded from stellar UV radiation where most S is expected to be in molecular form, by adding the abundances of all detected gas-phase S-bearing molecules, the resulting total S/H abundance is typically a factor of  $\sim 10^2$ – $10^3$  lower than the interstellar S/H abundance ( $< 1$  ppm; e.g., see Fuente et al. 2019). It is not yet clear in which form most S resides in molecular clouds. The S depletion appears to be environment-dependent (Fuente et al. 2023).<sup>1</sup> More recently, Ferrari et al. (2024) suggested that octasulfur S<sub>8</sub> may be an important S reservoir in molecular clouds, formed upon UV irradiation of H<sub>2</sub>S ices or electron irradiation of H<sub>2</sub>S and SO<sub>2</sub> ices (e.g., see Shingledecker et al. 2020, Mifsud et al. 2021, Cazaux et al. 2022). It is interesting to note that S<sub>8</sub> was recently detected in the Ryugu asteroidal samples (Aponte et al. 2023). If S<sub>8</sub> is responsible for the missing S in molecular clouds, it is expected to reveal its presence through three prominent bands at 53.5, 41.3 and 21.1  $\mu\text{m}$  (Ferrari et al. 2024).

### 1.4. Where Have All the Missing S Atoms Gone?

In the ISM, elements not seen in the gas phase must have been locked up in dust. For example, at least 95% of the interstellar Si, Mg and Fe elements are missing from the gas phase, indicating Si and Mg (and probably Fe as well) are locked up in silicate dust. The case for Fe is more complicated. The missing Fe could be depleted in Fe-rich silicate dust, iron oxides, iron sulfides (FeS) or pure solid iron. For the S elements missing from the gas phase, popular candidate solids are sulfides, including magnesium sulfide (MgS), silicon disulfide (SiS<sub>2</sub>) and, as mentioned above, FeS.

The formation of sulfide is likely to occur in carbon-rich circumstellar environments.

---

<sup>1</sup>By analyzing the atomic and ionized lines of S detected by the James Webb Space Telescope (JWST), Fuente et al. (2024) derived  $[\text{S}/\text{H}]_{\text{gas}} \approx 8$  ppm in the ionized and warm molecular phases toward the Orion Bar. Daffon et al. (2009) estimated the sulfur abundance based on the photospheric lines of a sample of ten B main-sequence stars of the Orion association and obtained  $\text{S}/\text{H} \approx 14.1 \pm 1.7$  ppm. This suggests a depletion of  $[\text{S}/\text{H}]_{\text{dust}} \approx 6$  ppm in the Orion Bar, implying a lower depletion of S/H in regions illuminated by young stars.

Lattimer et al. (1978) predicted the possible presence of various sulfur-bearing materials in carbon-rich systems. According to Zhukovska et al. (2008), MgS has priority in the cooling sequence of sulphur-bearing solid compounds. In principle, upon injection into the ISM, sulfides could be an component of interstellar dust.

However, MgS exhibits a prominent band at  $30\ \mu\text{m}$ . While such a  $30\ \mu\text{m}$  emission band is seen in asymptotic giant branch (AGB) stars, post-AGB stars and planetary nebulae, it has never been seen in the ISM. The  $30\ \mu\text{m}$  band is neither seen in absorption in heavily obscured interstellar sources toward the Galactic center nor in Wolf-Rayet stars. This suggests that MgS is not an interstellar dust component and the majority of the missing S is not depleted in MgS.

Similarly, the laboratory spectrum of  $\text{SiS}_2$  displays a prominent feature at  $\sim 22\ \mu\text{m}$  and a secondary feature at  $17\ \mu\text{m}$  (Nuth et al. 1985). As neither the  $22\ \mu\text{m}$  feature nor the  $17\ \mu\text{m}$  feature is seen in the ISM, either in absorption or emission,  $\text{SiS}_2$  cannot be an interstellar dust component and, thus  $\text{SiS}_2$  cannot be the sink of the missing S.

FeS has been identified in cometary dust sample and primitive meteorites (e.g., see Zolensky et al. 2006). Submicron-sized GEMS (glass with embedded metals and sulfides) have been identified in interplanetary dust particles (IDPs, Bradley 2003). Laboratory spectra of FeS solids show a strong band centered at  $\sim 23.5\ \mu\text{m}$ . While this band has been detected in emission in circumstellar disks surrounding several young stars and protoplanetary nebulae (PPNe) around evolved stars (Keller et al. 2002), it has not been seen in the ISM, either in emission or absorption. Therefore, FeS is also excluded as an important interstellar dust component.

In dense clouds, a possible explanation for the missing S is that, in addition to octasulfur  $\text{S}_8$  (see Shingledecker et al. 2020, Ferrari et al. 2024), S may be present in the icy mantles that coat interstellar dust grains.<sup>2</sup> However, ice carriers of S reservoir including solid OCS,  $\text{H}_2\text{S}$ , and  $\text{SO}_2$  can only account for a tiny fraction of the missing S (e.g., see Laas & Caselli 2019 and references therein). In Table 1 we summarize the interstellar S/H abundance as approximated by the photospheric abundance of the Sun, B stars and young F and G stars, proto-Sun, and the protosolar abundance argued by the GCE. Also tabulated is the

---

<sup>2</sup>Ammonium hydrosulfide ( $\text{NH}_4\text{SH}$ ) salt may also be present in dense clouds and in the upper layer of the coma in comets such as 67P/Churyumov-Gerasimenko (Altwegg et al. 2020). Very recently, Vitorino et al. (2024) performed experimental studies and demonstrated that  $\text{NH}_4\text{SH}$  salt could be formed at  $\sim 10\ \text{K}$  on grains from a mixture of  $\text{H}_2\text{S}$  and  $\text{NH}_3$ . Santos et al. (2024) also showed experimentally that S-bearing complex organic molecules could be formed from the interaction between  $\text{C}_2\text{H}_2$  molecules and SH radicals in interstellar ice mantles at  $\sim 10\ \text{K}$ .

S/H abundance missing from the gas phase in the diffuse ISM and in molecular clouds.

### 1.5. PAH as a Possible Sink for the Missing S

In §1.4 we have discussed that sulfides are unlikely the sink for the missing S in the ISM. Then, what else could the S reservoir be? As the smallest carbon component of the interstellar dust populations, polycyclic aromatic hydrocarbon (PAH) molecules are abundant and widespread in the Universe, as revealed by the ubiquitous detection of the aromatic IR emission (AIE) bands at 3.3, 6.2, 7.7, 8.6, 11.3 and 12.7  $\mu\text{m}$  (Léger & Puget 1984; Allamandola et al. 1985; Tielens 2008; Li 2020). Astronomical PAHs may not be pure aromatic compounds as strictly defined by chemists. Instead, PAH molecules in astronomical environments may include ring defects, aliphatic component (e.g., aliphatic sidegroups like methyl  $-\text{CH}_3$ ; see Yang & Li 2023a), substituents (e.g., N in place of C, see Hudgins et al. 2005, Mattioda et al. 2008; O in place of C, see Bauschlicher 1998; Fe in place of C, see Szczepanski et al. 2006), partial deuteration (e.g., see Allamandola et al. 1989, Draine 2006, Yang & Li 2023b), partial dehydrogenation and sometimes superhydrogenation (e.g., see Bernstein et al. 1996, Sandford et al. 2013, Yang et al. 2020).

Astronomical PAHs may also be sulfurated. Orthous-Daunay et al. (2010) performed XANES (X-ray Absorption Near Edge Structure) spectroscopic measurements of carbonaceous chondrites and identified several polycyclic aromatic sulfur heterocycles (PASHs; see Figure 1). If PASHs are present in the ISM in an appreciable quantity, it may not be impossible that PASHs may (at least partly) account for the missing S mystery. This motivates us to explore the IR emission spectra of interstellar PASHs.

To facilitate future searches for PASH molecules and quantitative determination of the PASH abundance so as to evaluate the potential of PASHs as a reservoir of the missing S in the ISM, especially in the JWST era, we perform for the first time a systematic calculation of the IR vibrational spectra of various PASH species. The structure of this paper is as follows. In §2 we briefly describe the computational methods and target molecules. We show in §3 the calculational results and derive the mean spectral properties (particularly the C–S band strengths) of PASH molecules (see §3.3). We then implement them in the astro-PAH model of Li & Draine (2001) and Draine & Li (2007) and discuss the astrophysical implications in §4. Finally, we summarize our major results in §5. This paper is largely concerned with the C–S band strengths of PASHs. In a subsequent paper we will model the IR emission spectra of PASH molecules of various sizes and compare with the astronomical spectra obtained with the Spitzer Space Telescope and JWST to quantitatively derive the amount of S/H depleted in PASHs.

## 2. Computational Methods and Target Molecules

PASHs have been widely studied by chemists, since the presence of heteroatoms of sulfur allows for diversifying the structures, reactivity and electronic properties (see Delaunay et al. 2016 and references therein). However, there is little study on PASHs in astronomy. As an illustrative investigation, in this work we consider target PASH molecules as shown in Figure 2. We focus on the heterocyclic organic sulfur, which has one or more benzene rings and also a five-membered ring with S incorporated. We consider PASH molecules with only one S atom incorporated. Those with more than one S atoms will be considered later. We start from one benzene ring all the way up to five.<sup>3</sup> Furthermore, we consider several isomers with different configurations. In total, we consider 18 molecules and their cations. The abbreviation of the naming of these molecules are referred following the National Institute of Standards and Technology (NIST) webbook.<sup>4</sup>

We use the Gaussian16 software (Frisch et al. 2016) to calculate the IR spectra of all of our target molecules. We employ the hybrid density functional theoretical (DFT) method (B3LYP) at the 6-311+G\*\* level to achieve the best compromise between accuracy and computational time (see Yang et al. 2013). The calculated frequencies are scaled with a factor of 0.9688 for all the vibrational modes (Borowski 2012). We note that in the literature sometimes different scaling factors were used for different modes (e.g., see Bauschlicher et al. 2018).

## 3. Results

### 3.1. Computational Accuracy

To test the accuracy of our calculation, we first compare the calculated IR spectra with those measured from laboratory. We apply this accuracy test to three molecules (BT, DBT and TT; see Figure 2 for molecule naming abbreviation) since experimental spectra are available for these three molecules.

---

<sup>3</sup>We note that these are fairly small molecules. Molecules with more than 20 C atoms (up to several hundreds and thousands of C atoms) are expected to emit in the JWST wavelength regime (see Croiset et al. 2016, Maragkoudakis et al. 2020, Draine et al. 2021). As we are mostly interested in the C–S band strengths of PASHs, it is not unreasonable to focus on small molecules. Also, large molecules are computationally expensive (and often not practical).

<sup>4</sup><https://webbook.nist.gov/chemistry/>

Figure 3 compares the computational spectra of BT, DBT and TT with their experimental spectra taken from the NIST webbook. As we do not have experimental information for the band intensities, we focus on the relative band strength comparison. The spectra are expressed as the molar (mol) extinction coefficient  $\varepsilon_{\tilde{\nu}}$  normalized to its peak value  $\varepsilon_{\tilde{\nu},\max}$ , where  $\tilde{\nu} \equiv \lambda^{-1}$  is the wavenumber. The full width at half maximum (FWHM) for all the calculational spectral bands is set to be  $16 \text{ cm}^{-1}$  to match the experimental spectra.

Figure 3 shows that we basically achieve consistency between calculational spectra and experimental spectra by employing the current theoretical level with the scaling factor given in Gaussian16. The peak wavelengths for the main vibrational modes, such as the C–H stretch at  $\sim 3100 \text{ cm}^{-1}$ , the C = C stretch at  $\sim 1400 \text{ cm}^{-1}$ , and the C–H out-of-plane bending at  $\sim 750 \text{ cm}^{-1}$ , match very well between calculations and experiments. A few minor features shown in the experimental spectra at  $\tilde{\nu} \sim 1500\text{--}2000 \text{ cm}^{-1}$  are absent in the calculational spectra, suggesting that they are not fundamentals but probably overtones or combinations instead.

Figure 3 demonstrates that our computational method can reasonably well reproduce the vibrational spectra of PASH molecules, both in wavelengths and in relative band strengths. In this regard, we will apply the computational method to all our 18 target molecules with B3LYP at level 6-311+G\*\*.

### 3.2. BT and its Cation

We show in Figure 4 the calculated IR spectra of BT and its cation. To illustrate the vibrational bands more clearly, we adopt a FWHM of  $16 \text{ cm}^{-1}$ . We clearly see in Figure 4 the C–H stretching band at  $3.3 \mu\text{m}$ , C–C stretch and C–H in-plane (ip) bending bands at  $\sim 6\text{--}10 \mu\text{m}$ , as well as the C–H out-of-plane (oop) bending bands at  $\sim 10\text{--}15 \mu\text{m}$ . For pure PAHs, it is well known that neutrals have stronger  $3.3$  and  $11.3 \mu\text{m}$  C–H bands, while cations contribute more to the C–C stretching and C–H ip bending bands in the wavelength range of  $\sim 6\text{--}10 \mu\text{m}$  (e.g., see Allamandola et al. 1999). However, for the PASH molecule BT, the situation seems different. While the BT cation ( $\text{BT}^+$ ) has much stronger C–C stretches than neutral BT, the  $3.3 \mu\text{m}$  C–H stretches are equally strong for BT ( $\sim 7.34 \text{ km mol}^{-1}$ ) and its ionic counterpart  $\text{BT}^+$  ( $\sim 5.84 \text{ km mol}^{-1}$ ). Also, the C–H oop bending bands at  $\sim 10\text{--}15 \mu\text{m}$  for BT is even weaker than that of  $\text{BT}^+$ .

To examine if such an effect is caused by sulfuration, we also show in Figure 4 the IR spectra of neutral and cationic indene, the *pure* PAH version (i.e., no sulfuration) of BT and  $\text{BT}^+$ . It is apparent that, just like typical PAH molecules, both the C–H stretch at  $3.3 \mu\text{m}$



and the C–H oop bending bands at  $\sim 10\text{--}15\ \mu\text{m}$  of neutral indene are much stronger than that of indene cation. This indicates that sulfuration significantly affects the C–H vibrational intensities of BT and BT<sup>+</sup>.

Figure 4 also shows that sulfuration also results in wavelength shifts for some of the vibrational bands. Generally, the incorporation of a metal element in PAHs will cause the shift of the central wavelength of the PAH bands, especially for the  $6.2\ \mu\text{m}$  C–C stretch. As a matter of fact, N-incorporated PAHs are usually resorted to explain the different central wavelength for the observed  $6.2\ \mu\text{m}$  emission band, and it is suggested that the N atom will cause the variation of the distribution of the electronic cloud (e.g., see Hudgins et al. 2004, Ricca et al. 2021). Experimental and computational studies have shown that the “ $6.2\ \mu\text{m}$ ” band of *pure* PAHs occurs at an appreciably longer wavelength incomparable with the astronomical  $6.2\ \mu\text{m}$  PAH band.<sup>5</sup>

The C–S bonds give rise to stretching vibrations, defined by the significant changes of the bond lengths. They generally occur in the  $\sim 9\text{--}16\ \mu\text{m}$  wavelength range. Meanwhile, there are also deformation vibrations, where the bond angles change, lying in the wavelength range of  $\sim 15\text{--}22\ \mu\text{m}$ . For illustration, we label the C–S stretch and deformation vibrations as “C–S” in Figure 4. As we are primarily interested in the C–S band strengths of PASHs, in the following we will focus on the C–S vibrations. For the C–C and C–H band strengths for “model” PASH molecules, we will *not* adopt that of the PASH target molecules computed here, instead, we will adopt that of astro-PAHs (Li & Draine 2001, Draine & Li 2007, Draine et al. 2021; see §4). The underlying assumption of this is that we assume that the presence of S atoms in a PAH molecule would not affect the C–C and C–H vibrations.

### 3.3. C—S Vibrational Spectra

We identify the C–S vibrations from the Gaussian output file, and read their frequencies and intensities for all the calculated target molecules and their cations. These results are tabulated in Tables 2 and 3 for the neutrals and cations, respectively.

The C–S stretches basically fall into the wavelength range of  $\sim 9\text{--}16\ \mu\text{m}$ , while the C–S deformation bands occur mainly in  $\sim 15\text{--}22\ \mu\text{m}$  except several cations show deformation bands at  $\sim 12\ \mu\text{m}$ . All the molecules considered here show relatively strong C–S stretch

---

<sup>5</sup>However, Ricca et al. (2024) recently argued that PAHs with edge defects could explain the central wavelength of the astronomical  $6.2\ \mu\text{m}$  PAH band using spectra computed with DFT without introducing PAHs that contain nitrogen within their ring structures.

around  $\sim 10 \mu\text{m}$  and  $\sim 12 \mu\text{m}$ , and several satellite features at  $\sim 10\text{--}15 \mu\text{m}$ . The deformation vibrations often peak at  $\sim 15 \mu\text{m}$  and  $\sim 20 \mu\text{m}$ . Generally, for both neutrals and cations the stretching modes have much larger intensities than the deformation modes. Both vibrational modes show a large diversity of wavelengths and intensities. The vibration modes often couple with each other. Especially in our target molecules, the five-membered ring where the S atom locates is attached to one or two benzene rings. Since several carbon atoms are shared by the five- and six-membered rings, the vibrations of these involved carbon atoms are often coupled. The degree of coupling is dependent on the configuration. Therefore, for different molecules, the number of C–S vibrational modes is different.

To illustrate the C–S vibrations, we show for each molecule the C–S vibration only spectrum as follows. We first convert the band strength ( $A_{\tilde{\nu}}$ ) given by the Gaussian outputs into absorption cross section ( $C_{\text{abs}}$ ) through

$$\frac{A_{\tilde{\nu}}}{\text{km mol}^{-1}} = 100 \times \int \frac{\varepsilon_{\tilde{\nu}}}{\text{L mol}^{-1} \text{cm}^{-1}} d\tilde{\nu} = 6.02 \times 10^{18} \times \int \frac{C_{\text{abs}}(\tilde{\nu})}{\text{cm}^2 \text{molecule}^{-1}} d\tilde{\nu} \quad , \quad (1)$$

where  $\varepsilon_{\tilde{\nu}}$  is the molar extinction coefficient and the integrations are performed over the band. For each molecule, we approximate each vibrational mode by a Drude function. For the  $j$ -th mode, let  $\gamma_j$  be the FWHM ( $\text{cm}^{-1}$ ),  $\tilde{\nu}_{0,j}$  be the peak wavenumber ( $\text{cm}^{-1}$ ), and  $A_j$  be the calculated intensity ( $\text{km mol}^{-1}$ ). The total absorption cross section is then expressed as

$$C_{\text{abs}}(\tilde{\nu}) = \sum_{j=1}^N \frac{1}{6.02 \times 10^{18}} \times A_{j,\tilde{\nu}} \times \frac{2\gamma_j}{\pi} \times \frac{1}{(\tilde{\nu} - \tilde{\nu}_{0,j}^2/\tilde{\nu})^2 + \gamma_j^2} \quad , \quad (2)$$

where  $C_{\text{abs}}$  in  $\text{cm}^2$  is the absorption cross section given in eq. 1 summed over  $N$  vibrational modes of a molecule. Using data from Tables 2 and 3, and taking  $\gamma_j = 30 \text{cm}^{-1}$  for all modes, we generate the absorption spectra ( $C_{\text{abs}}$ ) for each molecule and its cation, and plot in Figure 5.<sup>6</sup> When employing Drude functions to generate the spectra, we take a wavenumber range of  $0\text{--}3500 \text{cm}^{-1}$ , with a step size of  $0.2 \text{cm}^{-1}$ . To better compare the generated spectra with astronomical observations, we plot in the x-axis the wavelength in unit of  $\mu\text{m}$  in the range of  $5\text{--}30 \mu\text{m}$ , where all the C–S vibrational bands occur.

A close inspection of Figure 5 reveals that two cations, DBT+ and DN[23b23d]T+, have very different spectra. DBT+ has a very strong feature at  $11.2 \mu\text{m}$ , with an intensity of  $220.5 \text{km mol}^{-1}$ . It arises from the asymmetric stretch of C–S–C bonds in the five-membered ring. BN[21d]T, BN[23d]T, DN[12b12d]T, and DN[21b23d]T also have a similar configuration, with a substructure just the same as DBT but with more benzene rings attached.

---

<sup>6</sup>Observationally, the  $11.3 \mu\text{m}$  C–H out-of-plane bending feature has a mean width of  $\sim 0.36 \mu\text{m}$  (Draine & Li 2007). This corresponds to  $\sim 28 \text{cm}^{-1}$ .

They have similar vibrations, but occurring at shorter wavelength and with much smaller intensities. DBT+ also has a strong C–S deformation feature at  $28.3\ \mu\text{m}$ , with an intensity of  $47.65\ \text{km mol}^{-1}$ . This deformation, the strongest C–S deformation vibration among all of our target molecules, originates from the twisting of C–S–C bonds in the molecular plane. DN[23b23d]T+ shows two strong bands at  $9.76$  and  $15.67\ \mu\text{m}$ , both with intensities exceeding  $100\ \text{km mol}^{-1}$ . The  $9.76\ \mu\text{m}$  band also arises from the asymmetric stretch of the C–S–C bonds, while the  $15.67\ \mu\text{m}$  feature arises from the asymmetric stretch of the C–S–C bonds coupled with the deformation of the benzene ring. In view of the fact that the spectra of these two molecules are quite different from that of other molecules, especially they exhibit very strong vibrational intensities, we will exclude these two molecules (both neutral and cationic) in the following so that our results will not be biased by certain special molecules.

### 3.4. Mean C–S Vibrational Spectra

To highlight the C–S vibrational bands, we calculate the mean spectra obtained by averaging over all the target molecules illustrated in Figure 2 (except DBT and DN[23b23d]T). We show in Figure 6 the mean spectra for neutrals and cations, and it is apparent that the average spectra exhibit several bumps of different widths. To facilitate future quantitative comparison between these C–S vibrations with observations, we fit each of the mean spectra (for neutrals or cations) with a linear background plus several Lorentzian and Gaussian functions.<sup>7</sup> As illustrated in Figure 7, a combination of Lorentz and Gaussian functions closely reproduce the calculated mean spectra. We tabulate in Tables 4 and 5 the fitting results for the Lorentzian and Gaussian functions, including peak wavelengths, FWHMs, and intensities for neutrals and cations, respectively.

For neutral PASHs, we fit the mean spectrum with eight Lorentz functions plus two Gaussian functions. There are five relatively narrow bumps at wavelengths  $\lambda \lesssim 14\ \mu\text{m}$ , with FWHMs all  $\lesssim 0.8\ \mu\text{m}$ . These bumps are all pure C–S stretches. The other five bumps at wavelength of  $\lambda \gtrsim 14\ \mu\text{m}$  are mostly C–S deformation with very minor contributions from C–S stretch. The widths are relatively large, with FWHMs all exceeding  $\gtrsim 1.2\ \mu\text{m}$ . The large widths result from the broadening of the mixtures of neighbouring vibrational frequencies, suggesting a larger deviations in frequencies for such vibrational modes. Among all the C–S bands, the strongest is the one at  $\lambda \sim 12.44\ \mu\text{m}$ , with an integrated absorption cross section

---

<sup>7</sup>For the strong, sharp bands, we approximate them in terms of Lorentzian functions. In addition, there are a couple of broad “plateau” bands at  $\sim 18.6$  and  $20.9\ \mu\text{m}$  for neutrals and  $\sim 21.4\ \mu\text{m}$  for cations arising from mixtures of neighboring vibrations. For these broad bands, we approximate them by Gaussian functions (see Tables 4, 5).

of  $\sim 3.86 \times 10^{-25} \text{ cm}^3$  per S atom. The two neighboring bands at  $\lambda \lesssim 14.86$  and  $\sim 16.73 \mu\text{m}$  are prominent, with an integrated absorption cross section of  $\sim 2.16$  and  $2.09 \times 10^{-25} \text{ cm}^3$  per S atom, respectively.

For cations, we consider eight Lorentz functions and one Gaussian component for the fitting. The four C–S stretch bumps at wavelength  $\lesssim 14 \mu\text{m}$  are also very narrow, with FWHMs all below  $\lesssim 0.8 \mu\text{m}$ . Among them, the bump at  $\lesssim 9.95 \mu\text{m}$  is the strongest, with an integrated absorption cross section of  $\sim 6.60 \times 10^{-25} \text{ cm}^3$  per S atom. The five C–S deformation bands at wavelengths  $\gtrsim 15 \mu\text{m}$  are also very broad, just as that for neutrals. The FWHMs are mostly  $\sim 2.0 \mu\text{m}$ , except the very minor band at  $17.55 \mu\text{m}$ . Among them, the most prominent are the two bands at  $\sim 19.45 \mu\text{m}$  and  $\lesssim 25.93 \mu\text{m}$ , with an integrated absorption cross section of  $\lesssim 2.58$  and  $2.63 \times 10^{-25} \text{ cm}^3$  per S atom, respectively.

#### 4. Astrophysical Implications

Li & Draine (2001) and Draine & Li (2007) designed an “astro-PAH” model by empirically synthesizing  $C_{\text{abs}}(\text{PAH})$ , a set of absorption cross sections for PAHs that are consistent with spectroscopic observations of PAH emission in various astrophysical environments. Although the resulting “astro-PAH” absorption cross sections do not represent any specific material, they are generally consistent with laboratory data and approximate the actual absorption properties of the PAH mixture in astrophysical regions. For a sulfurated PAH molecule consisting of  $N_C$  C atoms and  $N_S$  S atoms, we approximate its absorption cross section  $C_{\text{abs}}(N_C, N_S)$  as a combination of the absorption cross section of pure PAH of the same size  $C_{\text{abs}}(N_C)$  and that of C–S vibrations:

$$C_{\text{abs}}(N_C, N_S) = C_{\text{abs}}(N_C) + N_S \times \left\{ \frac{C_{\text{abs}}(\text{PASH})}{N_S} \right\} . \quad (3)$$

where  $C_{\text{abs}}(N_C, N_S)$  is the absorption cross section of a sulfurated PAH molecule of  $N_C$  C atoms and  $N_S$  S atoms,  $C_{\text{abs}}(N_C)$  is the absorption cross section of a pure PAH molecule of  $N_C$  C atoms (see Li & Draine 2001, Draine & Li 2007, Draine et al. 2021), and  $C_{\text{abs}}(\text{PASH})/N_S$  is the average cross section of C–S vibrations (on a per S atom basis) calculated from eq.2 for all the target molecules. The resulting absorption cross sections are shown in Figures 8 and 9 for both neutrals and cations with  $N_C = 48$  and  $N_C = 96$  and various S atoms, i.e.,  $N_S = 0, 1, 3, 5$ .

Figures 8 and 9 clearly show that the C–S vibrational bands at  $\sim 10, 15$  and  $25 \mu\text{m}$  are rather strong and not mixed with the classical C–H and C–C bands of PAHs at  $3.3, 6.2, 7.7, 8.6, 11.3$  and  $12.7 \mu\text{m}$ . It is apparent that with even one S atom incorporated into a PAH

molecule, the C–S band at  $\sim 10 \mu\text{m}$  is appreciable for both neutrals and cations. Apparently, the  $\sim 10 \mu\text{m}$  C–S band would be the most promising tracer for interstellar PASH. On the other hand, the C–S band at  $15 \mu\text{m}$  is broader and less significant. It requires a larger degree of sulfuration, e.g.,  $N_S = 3$ , for the  $15 \mu\text{m}$  C–S band to be clearly seen in the vibrational spectra of neutrals. This band is much weaker in cations and requires  $N_S = 5$  for the  $15 \mu\text{m}$  band to be seen. The  $25 \mu\text{m}$  bands in both neutrals and cations are quite weak.

To account for the 3.3, 6.2, 7.7, 8.6, 11.3 and  $12.7 \mu\text{m}$  emission observed in the Galactic diffuse ISM, Li & Draine (2001) and Draine & Li (2007) found that an amount of  $\text{C}/\text{H} \approx 40\text{--}60$  ppm is required to be locked up in PAHs. Let’s take an intermediate value of  $[\text{C}/\text{H}]_{\text{PAH}} = 50$  ppm and assume a single PAH size of  $N_C$  C atoms for the entire interstellar PAH population which depletes a total C/H abundance of  $[\text{C}/\text{H}]_{\text{PAH}}$ . Then, such a PAH population containing  $N_S$  S atoms would lock up a total S/H abundance of  $[\text{S}/\text{H}]_{\text{PAH}} = [\text{C}/\text{H}]_{\text{PAH}} \times (N_S/N_C)$ . As shown in Figure 8, PAH molecules of  $N_C = 48$  C atoms and  $N_S = 1$  S atom exhibit a noticeable C–S band at  $10 \mu\text{m}$ . For the Galactic ISM, Li & Draine (2001) derived a mean PAH size of  $N_C \approx 100$ . In this case,  $N_S = 1$  corresponds to  $[\text{S}/\text{H}]_{\text{PAH}} \approx 0.5$  ppm.

We note that, while the IR spectra of several regions in the Orion Bar recently obtained by the *Mid-Infrared Instrument* (MIRI) on board JWST (Chown et al. 2024) do not seem to show any emission at  $10 \mu\text{m}$ , the *Spitzer Infrared Spectrograph* (IRS) spectra of the Galactic reflection nebulae NGC 2023 and NGC 7023 do exhibit a weak band at  $10.1 \mu\text{m}$  (see Werner et al. 2004, Sellgren et al. 2010).<sup>8</sup> We should also note that the  $10 \mu\text{m}$  bands shown in Figures 8 and 9 are the absorption cross section of the C–S stretch and should not be *readily* used to estimate the amount of S/H depleted in PAHs by *directly* comparing with the astronomical spectra. To quantitatively explore the amount of S/H locked up in PASHs, we have to fold the absorption cross sections of PASHs with the starlight radiation field to model the vibrational excitation of PASHs and calculate their IR emission spectra. This will be investigated in a subsequent paper.

Finally, we note that the detectability of the  $10 \mu\text{m}$  C–S band could be affected by the broad silicate absorption band centered at  $9.7 \mu\text{m}$ . In external galaxies such as M82, NGC 253 and Circinus, their *Spitzer*/IRS spectra show a strong  $9.7 \mu\text{m}$  silicate absorption band (see Sturm et al. 2000). The  $10 \mu\text{m}$  C–S band of PASHs could be hidden by the silicate absorption band even if PASHs are present. This could also be true in the Orion Bar which subjects to a substantial amount of extinction (see Fuente et al. 2024). In the subsequent

---

<sup>8</sup>Werner et al. (2004) attributed the weak  $10.1 \mu\text{m}$  emission band seen in NGC 7023 to the C–H oop bending modes of PAHs (Hony et al. 2001).

paper we will also investigate this in detail, in combination with the latest available JWST spectroscopic data.

## 5. Summary

Despite its biogenic and astrochemical importance, S-containing molecules and ices in molecular clouds are far below expected from the interstellar S abundance of  $[S/H]_{\text{ISM}} \approx 22.4$  ppm. In the diffuse ISM, although it was previously thought that S is not depleted, recent observations suggest that an appreciable portion of the interstellar S in the diffuse ISM is also missing from the gas. With common sulfides like MgS, FeS and SiS<sub>2</sub> excluded as a major S reservoir, we have examined the possibility that the missing S may have partly been locked up in PASHs—polycyclic aromatic sulfur heterocycles by computing the IR vibrational spectra of 18 representative PASH species. We find that these molecules exhibit a prominent, stand-alone C–S stretching band at  $\sim 10 \mu\text{m}$  which is detectable by JWST if several ppm of S/H is depleted in PASHs. A weak emission band at  $10.1 \mu\text{m}$  has already been seen in the *Spitzer*/IRS spectra of NGC 2023 and NGC 7023. Future JWST observations will allow one to quantitatively examine if PASH could account for some portions of the S elements missing from the gas phase.

We dedicate this paper to the memory of Edward B. Jenkins with whom we discussed the possible depletion routes of S during the BruceFest in Florence, Italy on October 30 – November 3, 2023. Ed was an active participant in the biweekly Interstellar Medium Seminar one of us (AL) once organized and benefited much in Princeton in 1999–2002. We thank the anonymous referees for helpful comments and suggestions. We thank B.M. Broderick, B.T. Draine, and E.F. van Dishoeck for stimulating discussions. XJY and HLJ are supported in part by NSFC 12333005 and 12122302 and CMS-CSST-2021-A09.

## REFERENCES

- Allamandola, L. J., Hudgins, D. M., & Sandford, S. A. 1999, *ApJ*, 511, L115
- Allamandola, L. J., Tielens, A. G. G. M., & Barker, J. R. 1985, *ApJ*, 290, L25
- . 1989, *ApJS*, 71, 733
- Altwegg, K., Balsiger, H., Hänni, N., et al. 2020, *Nature Astronomy*, 4, 533
- Anderson, D. E., Bergin, E. A., Maret, S., & Wakelam, V. 2013, *ApJ*, 779, 141

- Aponte, J. C., Dworkin, J. P., Glavin, D. P. 2023, EP&S, 75, 28
- Asplund, M., Grevesse, N., Sauval, A. J., & Scott, P. 2009, ARA&A, 47, 481
- Bauschlicher, Charles W., J. 1998, Chemical Physics, 233, 29
- Bauschlicher, C. W., Ricca, A., Boersma, C., et al. 2018, ApJS, 234, 32
- Bernstein, M. P., Sandford, S. A., & Allamandola, L. J. 1996, ApJL, 472, L127
- Borowski, P. 2012, JPCA, 116, 3866
- Bradley, J.P. 2003. Interplanetary dust particles. In Meteorites, Comets, and Planets, ed. A.M. Davis, Treatise on Geochemistry, vol. 1, Oxford: Elsevier-Pergamon, 690
- Cazaux, S., Carrascosa, H., Caro, G. M., et al. 2022, A&A, 657, 100
- Chiappini, C., Romano, D., & Matteucci, F. 2003, MNRAS, 339, 63
- Chown R., Sidhu, A., Peeters, E., et al. 2024, A&A, 685, 75
- Croiset, B. A., Candian, A., Berné, O., & Tielens, A. G. G. M. 2016, A&A, 590, 26
- Dafon, S., Cunha, K., de la Reza, R., Holtzman, J., & Chiappini, C. 2009, AJ, 138, 1577
- Delaunay, W., Szűcs, R., Pascal, S., et al. 2016, Dalton Transactions, 45, 1896
- Draine, B. T. 2006, in ASP Conf. Ser. 348, Astrophysics in the Far Ultraviolet: Five Years of Discovery with FUSE, ed. G. Sonneborn et al. (San Francisco, CA: ASP), 58
- Draine, B. T., & Li, A. 2007, ApJ, 657, 810
- Draine B. T., Li A., Hensley B. S., et al. 2021, ApJ , 917, 3
- Dutrey, A., Guilloteau, S., & Guelin, M. 1997, A&A, 317, L55
- Ferrari, P., Berden, G., Redlich, B., Waters, L. B. F. M., & Bakker, J. M. 2024, Nature Communication, 15, 5928
- Frisch, M. J., Trucks, G. W., Schlegel, H. B., et al. 2016, Gaussian 16, Gaussian, Inc. Wallingford, CT
- Fuente, A., Navarro, D., Caselli, P., et al. 2019, A&A, 624, 105
- Fuente, A., Rivière-Marichalar, P., Beitia-Antero, L., et al. 2023, A&A, 670, 114

- Fuente, A., Roueff, E., Le Petit, F., et al. 2024, *A&A*, 687, A87
- Hensley, B. S., & Draine, B. T. 2021, *ApJ*, 906, 73
- Hily-Blant, P., Pineau des Forêts, G., Faure, A., & Lique, F. 2021, *A&A*, 658, 168
- Hony, S., Van Kerckhoven, C., Peeters, E., et al. 2001, *A&A*, 370, 1030
- Howk, J. C., Sembach, K. R., & Savage, B. D. 2006, *ApJ*, 637, 333
- Hudgins, D. M., Allamandola L.J., 2004, in Witt A. N., Clayton G. C., Draine B. T., eds, ASP Conf. Ser. Vol. 309, *Astrophysics of Dust*. Astron. Soc. Pac., San Francisco, p. 665
- Hudgins, D. M., Bauschlicher Jr, C. W., & Allamandola, L.J. 2005, *ApJ*, 632, 316
- Jenkins, E. B. 2009, *ApJ*, 700, 1299
- Keller, L. P., Hony, S., Bradley, J. P., et al. 2002, *Nature*, 417, 148
- Krijt, S., Kama, M., McClure, M., et al. 2023, *Protostars and Planets VII*, ASP Conference Series, Vol. 534, Proceedings of a conference held 10-15 April 2023 at Kyoto, Japan. Edited by Shu-ichiro Inutsuka, Yuri Aikawa, Takayuki Muto, Kengo Tomida, and Motohide Tamura. San Francisco: Astronomical Society of the Pacific, p.1031
- Laas, J. C., & Caselli, P. 2019, *A&A*, 624, 108
- Lattimer, J. M., Schramm, D. N., & Grossman, L. 1978, *ApJ*, 219, 230
- Le Gal, R., Öberg, K. I., Loomis, R. A., Pegues, J., & Bergner, J. B. 2019, *ApJ*, 876, 72
- Léger, A., & Puget, J. 1984, *A&A*, 137, L5
- Li, A., & Draine, B. T. 2001, *ApJ*, 554, 778,
- Li, A. 2020, *Nature Astronomy*, 4, 339
- Lodders, K. 2003, *ApJ*, 591, 1220
- McClure, M. K., Rocha, W. R. M., Pontoppidan, K. M., et al. 2023, *Nature Astronomy*, 7, 431
- Maragkoudakis, A., Peeters, E., & Ricca, A. 2020, *MNRAS*, 494, 642
- Mattioda, A. L., Rutter, L., Parkhill, J., et al. 2008, *ApJ*, 680, 1243



- Mifsud, D. V., KaÅuchová, Z., Herczku, P., et al. 2021, SSRv, 217, 14
- Nuth, J. A., Moseley, S. H., Silverberg, R. F., Goebel, J. H., & Moore, W. J. 1985, ApJL, 290, L41
- Orthous-Daunay, F.-R., Quirico, E., Lemelle, L., et al. 2010, EPSL, 300, 321
- Prasad, S. S., & Huntress, W. T., J. 1982, ApJ, 260, 590
- Przybilla, N., Nieva, M.-F., & Butler, K. 2008, ApJ, 688, L103
- Ricca A., Boersma C., & Peeters E., 2021, ApJ, 923, 202
- Ricca, A., Roser, J. E., Boersma, C., et al. 2024, ApJ, 968, 128
- Sandford, S. A., Bernstein, M. P., & Materese, C. K. 2013, ApJS, 205, 8
- Santos, J. C., Enrique-Romero, J., Lamberts, T., Linnartz, H., & Chuang, K. 2024, arxiv2407.09730
- Sellgren, K., Werner, M. W., Ingalls, J. G., et al. 2010, ApJ, 722, L54
- Shingledecker, C. N., Lamberts, T., Laas, J. C., et al. 2020, ApJ, 888, 52
- Sturm, E., Lutz, D., Tran, D., et al. 2000, A&A, 358, 481
- Szczepanski, J., Wang, H., Vala, M., et al. 2006, ApJ, 646, 666
- Tielens, A. G. G. M. 2008, ARA&A , 46, 289
- Vitorino, J., Loison, J.-C., Wakelam, V., Congiu, E., & Dulieu, F. 2024, MNRAS, in press
- Wakelam, V., Caselli, P., Ceccarelli, C., Herbst, E., & Castets, A. 2004, A&A, 422, 159
- Werner, M. W., Uchida, K. I., Sellgren, K., et al. 2004, ApJS, 154, 309
- White, B., & Sofia, U. 2011, in Am. Astron. Soc. Meeting Abstracts #218, 129.23
- Yang, X. J., Glaser, R., Li, A., & Zhong, J. X. 2013, ApJ, 776, 110
- Yang, X. J., Li, A., & Glaser, R. 2020, ApJS, 247, 1
- Yang, X. J., & Li, A. 2023a, ApJS, 268, 50
- Yang, X. J., & Li, A. 2023b, ApJS, 268, 12
- Zhou, S., Evans, N. J., Koempe, C., & Walmsley, C. 1993, ApJ, 404, 232

Zhukovska, S., & H.-P., G. 2008, A&A, 486

Zolensky, M.E., Zega, T.J., Yano, H., et al. 2006, Science, 314, 1735

Zuo, W. B., Li, A., & Zhao, G. 2021, ApJ, 257, 63

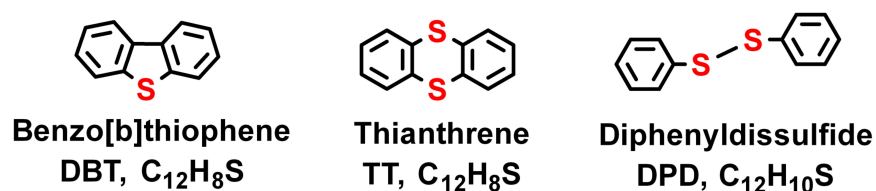


Fig. 1.— Structures of PASH molecules identified in meteorites.

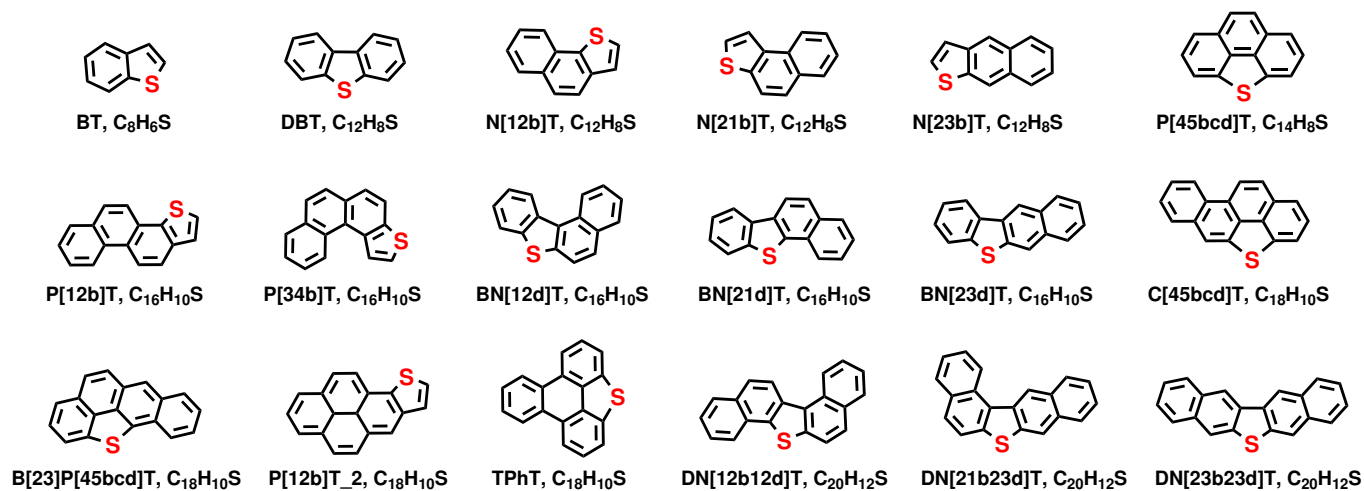


Fig. 2.— Structures of all the target molecules considered in this work.

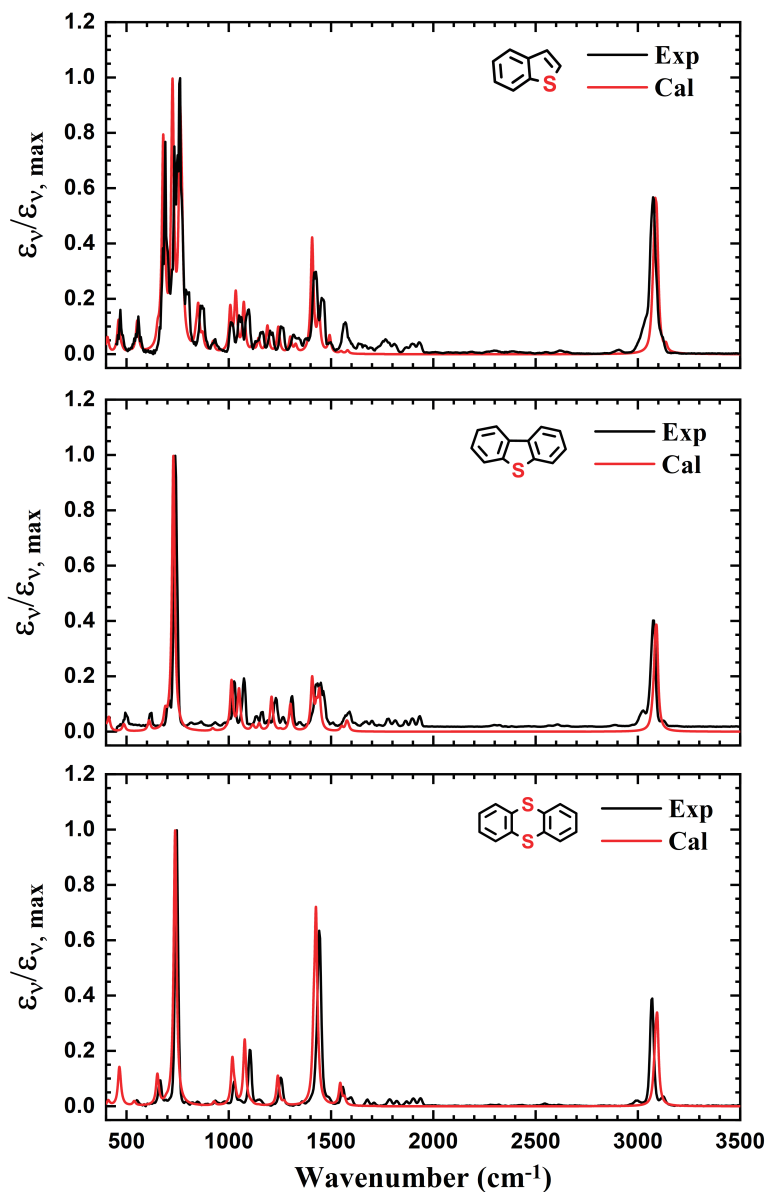


Fig. 3.— Comparison of the experimental (black solid lines) and calculational (red solid lines) spectra for BT (upper panel), DBT (middle) and TT (bottom). The experimental spectra are taken from the NIST webbook. The frequencies of the calculated spectra are scaled with a factor 0.9688, and an FWHM of  $16 \text{ cm}^{-1}$  is assigned. For comparison, both the experimental and calculated spectra are normalized to their maxima due to the lack of experimental information on the intensities of these molecules.

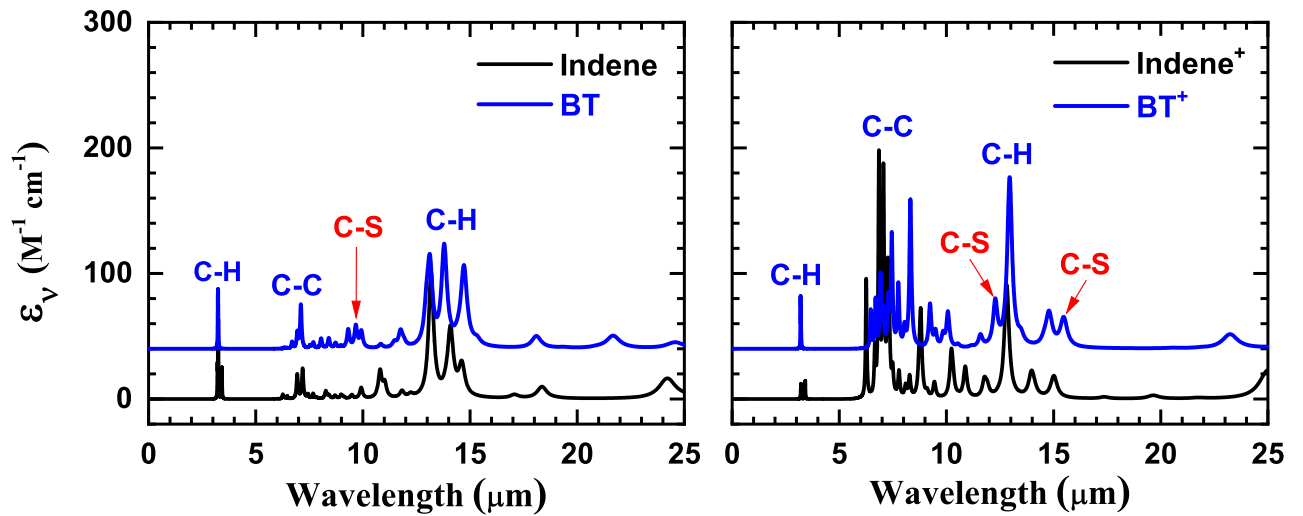


Fig. 4.— Calculated spectra of BT (left panel) and BT<sup>+</sup> (right panel). The origins of the main features are labeled, including C–H, C–C, and C–S bonds. The frequencies of the calculated spectra are scaled with a factor 0.9688, and a FWHM of  $16 \text{ cm}^{-1}$  is assigned.

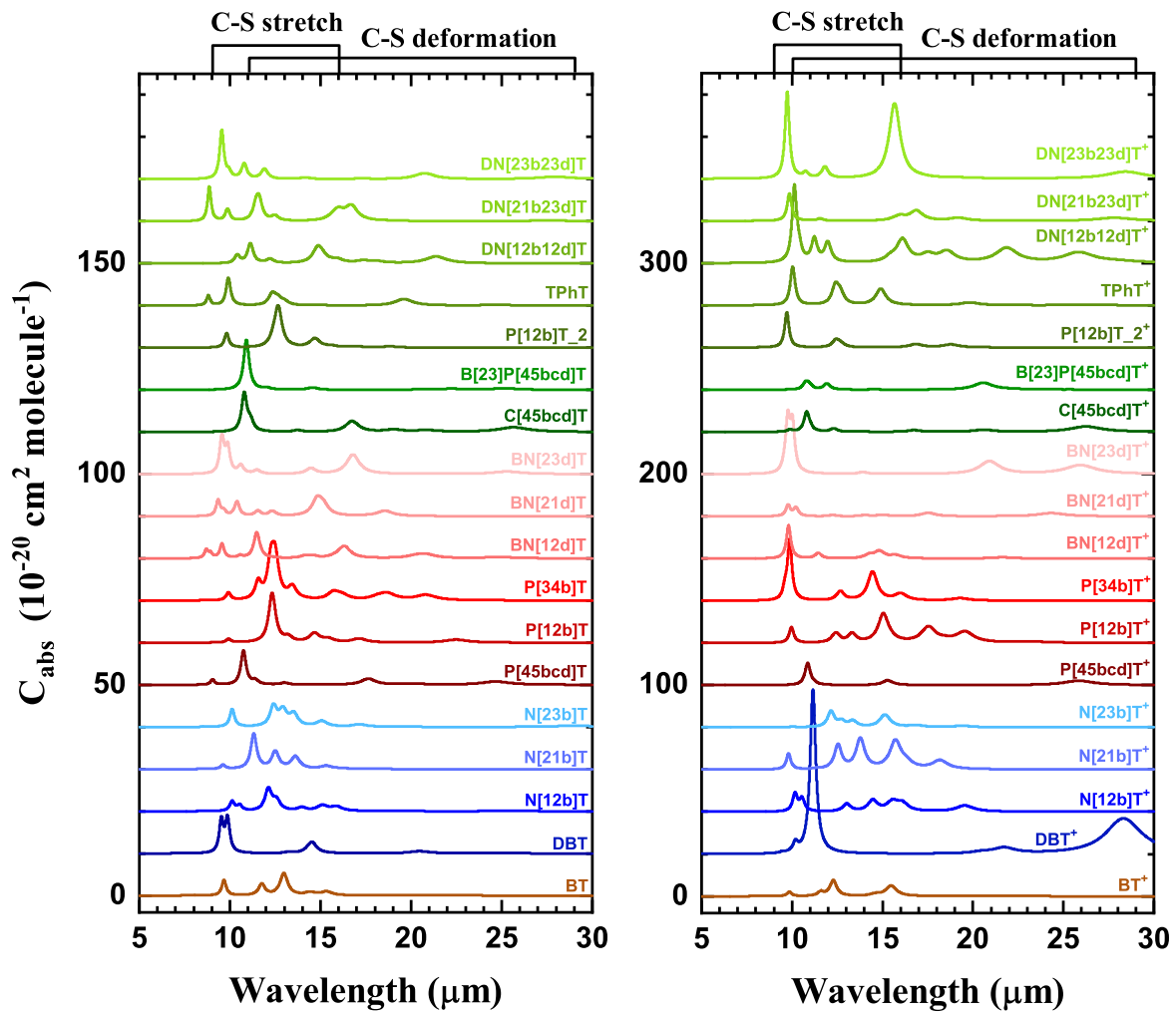


Fig. 5.— Calculated spectra of all the target molecules (left panel; see Figure 2) and their cations (right panel). The wavelength ranges for the main vibrational bands are marked on top.

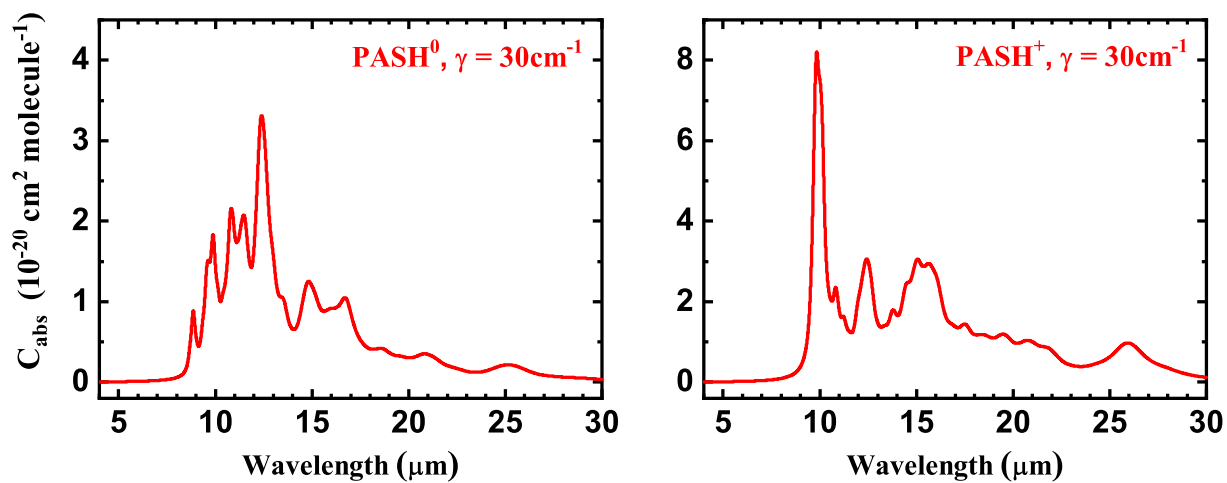


Fig. 6.— Average spectra of the C–S vibrations of all the target PASH neutrals (left panel) and cations (right panel) except DBT, DN[23b23d]T and their cations.

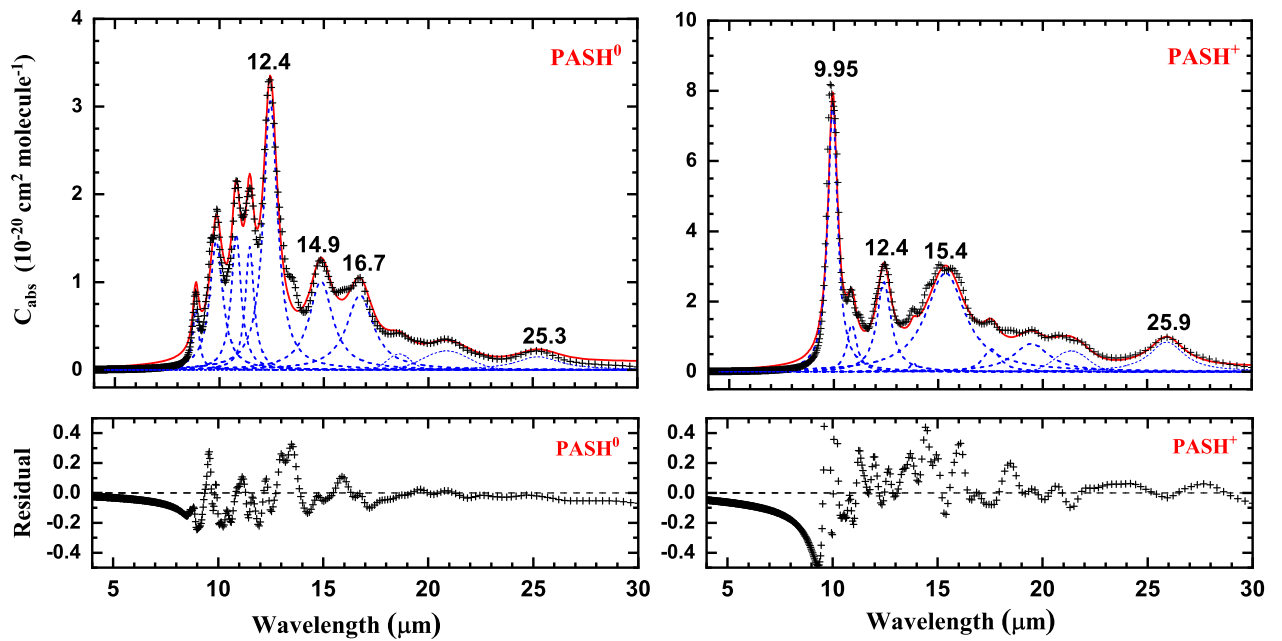


Fig. 7.— Fitting the average C–S vibrational spectra of neutrals (left panel) and cations (right panel) in terms of a linear background and several Drude and/or Gaussian functions. The central wavelengths (in  $\mu\text{m}$ ) of the most prominent bands are marked. Also shown are the fitting residuals obtained by subtracting the fitted spectra from the original spectra.



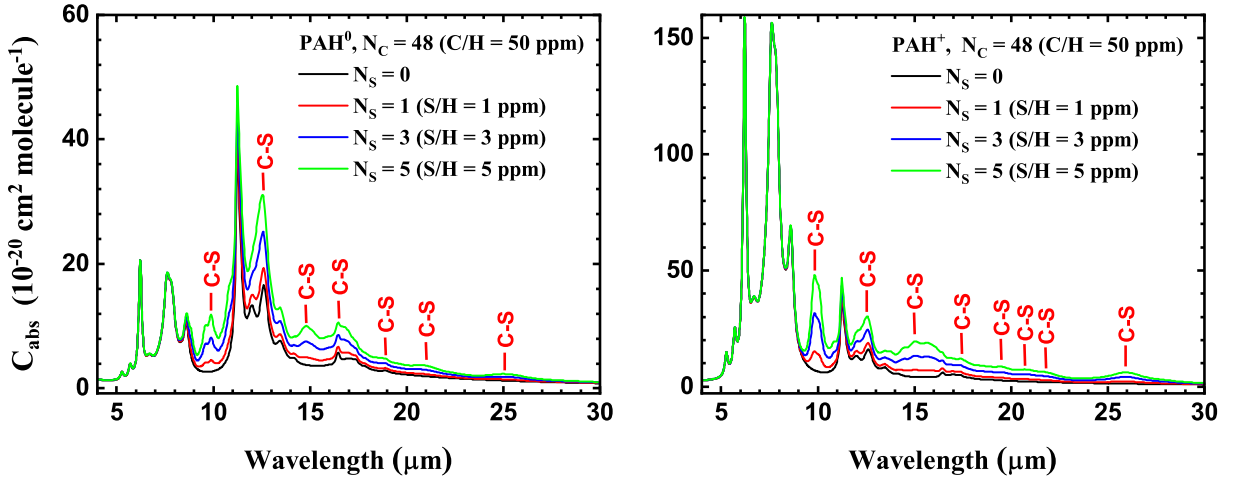


Fig. 8.— Absorption cross sections for a S-containing PAH molecule of 48 C atoms (left panel) and its cation (right panel). As described in eq. 3, the absorption cross sections are obtained by adding the C–S vibrational bands of various S atoms ( $N_S = 0, 1, 3,$  and  $5$ ) to that of astro-PAHs of Draine & Li (2007). Assuming the interstellar PAH population consumes a total C/H abundance of  $[C/H]_{\text{PAH}} = 50$  ppm and has a single size of  $N_C = 48$  C atoms, then,  $N_S$  S atoms correspond to a total S/H depletion of  $[S/H]_{\text{PAH}} = [C/H]_{\text{PAH}} \times (N_S/N_C) \approx N_S$  ppm.

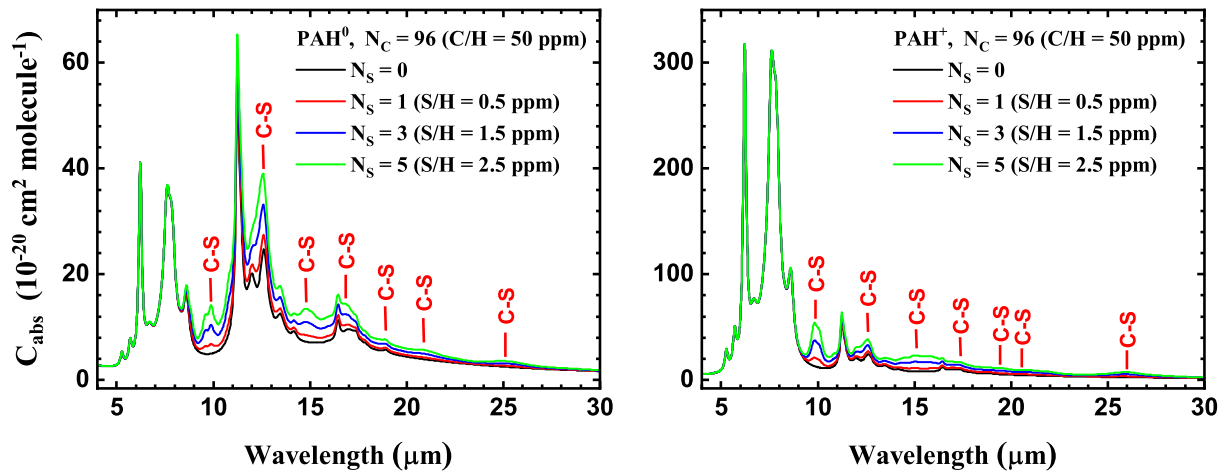


Fig. 9.— Same as Figure 8 but for a large molecule with  $N_C = 96$ .

Table 1: Interstellar Sulfur Abundance

Elemental Abundance	B and F, G Stars <sup>a</sup>	Sun <sup>b</sup>	Proto-Sun <sup>c</sup>	Proto-Sun +GCE <sup>d</sup> (ppm)	Diffuse ISM (ppm)		Molecular Clouds (ppm)	
	(ppm)	(ppm)	(ppm)		Gas <sup>e</sup>	Dust <sup>f</sup>	Gas <sup>g</sup>	Dust <sup>h</sup>
S/H	14.5±1.0	16.2±1.3	18.2±1.7	22.4±1.7	9.6	12.8	< 1	22.4

*a:* Asplund et al. 2009

*b:* Przyllilla et al. 2008

*c:* Lodders 2003

*d:* Chiappini et al. 2003

*e:* Draine & Hensley 2021

*f:* Our adopted sulfur abundance of 22.4 ppm minus that in the gas phase

*g:* Fuente et al. 2019

*h:* Our adopted sulfur abundance of 22.4 ppm minus that in the gas phase

Table 2:: Frequencies and Intensities of the C–S Vibrational Modes of Neutral PASHs

Molecule	C–S Stretch		C–S Deformation	
	Wavelength ( $\mu\text{m}$ )	Intensity ( $\text{km mol}^{-1}$ )	Wavelength ( $\mu\text{m}$ )	Intensity ( $\text{km mol}^{-1}$ )
BT	9.67	10.42	15.33	2.46
	11.76	7.52	19.37	0.33
	12.97	14.73	20.94	0.39
	14.43	1.97		
DBT	9.51	11.33	20.42	1.28
	9.54	10.55	20.74	0.23
	9.87	22.54	24.50	0.24
	13.21	0.65		
	14.44	1.20		
N[12b]T	10.12	6.41	15.10	3.54
	10.54	3.71	15.87	2.90
	12.12	14.65	18.29	0.34
	12.57	6.80	25.48	0.25
	13.96	2.17		
N[21b]T	9.62	2.93	15.31	1.99
	11.31	23.65	16.15	0.38
	12.50	11.47	18.09	0.04
	13.61	8.17		
N[23b]T	10.12	11.94	17.15	1.61
	12.40	13.41	18.92	0.21
	12.93	10.21	28.96	0.85
	13.52	8.14		
	15.07	3.71		
P[45bcd]T	9.04	3.54	13.01	1.30
	10.75	22.75	15.18	0.39
	11.40	2.66	17.64	4.07
	14.03	0.19	19.80	0.23
			20.18	0.60
		24.52	0.96	

Molecule	C-S Stretch		C-S Deformation	
	Wavelength ( $\mu\text{m}$ )	Intensity ( $\text{km mol}^{-1}$ )	Wavelength ( $\mu\text{m}$ )	Intensity ( $\text{km mol}^{-1}$ )
			24.77	1.25
P[12b]T	9.92	2.42	15.40	2.37
	12.33	32.40	17.13	2.57
	12.37	0.89	17.91	0.03
	13.22	3.19	22.48	2.01
	14.66	5.92		
P[34b]T	9.92	5.01	11.56	11.33
	13.44	8.15	12.26	23.68
			12.50	25.49
			14.16	0.25
			15.70	4.78
			16.06	1.16
			16.24	2.03
			18.14	1.71
			18.67	4.17
		19.54	0.17	
		20.81	3.51	
BN[12d]T	8.69	5.50	14.54	1.52
	8.92	3.45	15.77	0.58
	9.56	9.79	16.31	8.10
	10.57	1.53	20.23	1.12
	11.48	17.51	20.77	2.57
	12.32	0.14	24.84	0.86
	14.12	1.32		
BN[21d]T	9.35	10.82	11.54	3.36
	9.66	3.18	17.39	0.16
	10.39	9.68	18.55	3.53
	12.33	3.39	20.82	0.05
	13.95	0.12	24.18	0.02
	14.80	10.40		
BN[23d]T	9.54	18.27	11.50	2.57
	9.62	7.58	14.47	3.86

Molecule	C-S Stretch		C-S Deformation	
	Wavelength ( $\mu\text{m}$ )	Intensity ( $\text{km mol}^{-1}$ )	Wavelength ( $\mu\text{m}$ )	Intensity ( $\text{km mol}^{-1}$ )
BN[23d]T	9.88	17.15	16.79	13.02
	10.60	5.64	20.78	0.34
			25.28	1.70
C[45bcd]T	10.79	25.80	13.74	1.12
	11.14	6.29	16.71	5.19
			16.82	2.17
			19.03	1.46
			20.59	0.53
			21.09	0.63
			25.64	3.10
B[23]P[45bcd]T	10.88	14.17	20.51	0.28
	10.93	20.04	22.21	0.71
	12.04	1.08	25.15	0.94
	14.56	1.57		
P[12b]T <sub>2</sub>	9.82	9.71	16.98	0.68
	12.40	4.15	18.83	0.77
	12.67	26.67		
	14.69	5.92		
	15.58	0.95		
TPhT	8.81	6.67	12.64	3.97
	9.91	18.76	13.00	2.38
	12.33	7.47	19.60	4.42
	14.77	0.53	24.73	0.47
DN[12b12d]T	10.41	5.50	14.85	9.90
	11.13	13.32	17.34	1.46
	12.21	2.74	18.09	1.19
	15.10	2.68	21.37	4.63
	15.91	2.31		
DN[21b23d]T	8.86	23.09	15.65	1.27
	9.87	8.06	15.97	6.55
	11.43	8.79	16.70	9.71
	11.61	13.01	18.98	0.23

Molecule	C-S Stretch		C-S Deformation	
	Wavelength ( $\mu\text{m}$ )	Intensity ( $\text{km mol}^{-1}$ )	Wavelength ( $\mu\text{m}$ )	Intensity ( $\text{km mol}^{-1}$ )
	12.49	3.15	27.57	0.60
	9.55	32.73	14.15	1.12
	9.95	3.93	17.24	0.44
DN[23b23d]T	10.78	10.07	19.44	0.01
	11.90	6.80	20.75	4.04
			27.94	1.58

Table 3:: Same as Table 2 but for Cationic PASHs

Molecule	C-S Stretch		C-S Deformation	
	Wavelength ( $\mu\text{m}$ )	Intensity ( $\text{km mol}^{-1}$ )	Wavelength ( $\mu\text{m}$ )	Intensity ( $\text{km mol}^{-1}$ )
BT <sup>+</sup>	9.84	5.83	15.47	13.67
	11.59	5.41	21.90	0.19
	12.28	20.84		
	14.58	2.49		
DBT <sup>+</sup>	9.49	1.64	20.48	2.18
	10.19	12.46	21.72	7.63
	11.15	220.54	28.32	47.63
	14.26	0.49		
N[12b]T <sup>+</sup>	14.46	14.76	10.16	23.79
			10.55	16.87
			13.02	10.11
			15.55	11.87
			16.09	10.42
N[21b]T <sup>+</sup>	9.80	21.31	15.71	36.99
	11.33	0.81	16.32	6.59
	12.54	32.11	18.18	11.53
	13.77	40.46		
N[23b]T <sup>+</sup>	10.04	0.95	16.60	0.80
	12.15	21.09	17.02	1.63
	12.73	7.22	19.40	2.02
	13.36	7.89		
	15.13	16.84		
P[45bcd]T <sup>+</sup>	10.86	29.59	20.19	0.37
	11.23	1.08	25.84	5.92
	15.28	6.38		
P[12b]T <sup>+</sup>	9.97	21.01	15.49	1.61
	12.28	3.17	17.54	20.33
	12.45	10.75	18.45	2.36
	13.32	11.57	19.55	13.95



Molecular	C-S Stretch		C-S Deformation	
	Wavelength ( $\mu\text{m}$ )	Intensity ( $\text{km mol}^{-1}$ )	Wavelength ( $\mu\text{m}$ )	Intensity ( $\text{km mol}^{-1}$ )
	15.05	38.09	23.16	1.71
P[34b]T <sup>+</sup>	9.61	13.37	15.99	5.66
	9.87	79.21	16.03	3.18
	12.67	12.13	19.29	3.15
	14.45	38.65		
BN[12d]T <sup>+</sup>	9.80	43.65	21.63	1.58
	9.93	0.86		
	11.45	7.47		
	14.26	4.59		
	14.83	9.35		
	15.72	4.09		
BN[21d]T <sup>+</sup>	9.69	0.40	17.52	4.62
	9.78	14.73	21.43	0.14
	10.22	11.04	24.33	4.33
	12.24	1.67		
	14.03	1.47		
	15.01	2.02		
BN[23d]T <sup>+</sup>	9.56	4.83	15.92	0.42
	9.76	68.31	20.91	17.14
	10.02	63.42	25.94	11.85
	10.57	0.56		
	11.49	0.47		
	13.92	2.48		
C[45bcd]T <sup>+</sup>	9.88	2.94	16.74	2.28
	10.81	26.04	20.58	2.76
	11.01	3.11	26.25	7.26
	12.30	4.36		
	13.64	0.95		
B[23]P[45bcd]T <sup>+</sup>	10.76	9.11	20.56	9.33
	10.95	5.97	22.14	0.54
	11.93	8.18	25.68	0.17
	14.55	0.39		

Molecular	C-S Stretch		C-S Deformation	
	Wavelength ( $\mu\text{m}$ )	Intensity ( $\text{km mol}^{-1}$ )	Wavelength ( $\mu\text{m}$ )	Intensity ( $\text{km mol}^{-1}$ )
P[12b]T <sub>2</sub> <sup>+</sup>	9.71	47.36	15.52	0.14
	12.42	9.76	16.86	4.42
P[12b]T <sub>2</sub> <sup>+</sup>	12.70	4.22	18.77	3.90
	14.95	0.43		
TPhT <sup>+</sup>	10.02	40.85	19.81	3.65
	10.09	12.65	26.30	0.72
	12.40	24.61		
	12.67	13.84		
	14.90	21.82		
DN[12b12d]T <sup>+</sup>	10.13	100.66	17.50	9.59
	10.40	13.49	18.56	14.14
	11.23	30.79	21.86	19.39
	11.97	26.20	25.84	13.73
	15.45	5.64	27.98	1.63
DN[21b23d]T <sup>+</sup>	16.10	30.43		
	9.85	36.79	15.66	1.42
	10.75	0.39	16.87	13.15
	11.55	2.88	19.19	3.91
DN[23b23d]T <sup>+</sup>	15.98	5.36	27.81	4.13
	9.73	116.28	17.06	0.40
	10.75	7.06	19.29	0.63
	11.82	15.24	28.43	9.32
	15.67	101.15		

Table 4: Parameters for Fitting the C–S Bands of Neutral PASHs. The band intensities ( $\text{cm}^3$  per S atom) is the absorption cross section of the band integrated over wavelength (i.e.,  $\int_{\text{band}} C_{\text{abs}}(\lambda)d\lambda$ )

Wavelength ( $\mu\text{m}$ )	FWHM ( $\mu\text{m}$ )	Intensity ( $10^{-25} \text{cm}^3$ per S)
8.87	0.35	0.38
9.85	0.75	1.73
10.80	0.56	1.36
11.45	0.50	1.10
12.44	0.80	3.86
14.86	1.36	2.16
16.73	1.56	2.09
18.60*	1.29	0.25
20.85*	2.56	0.59
25.25	2.56	0.60

\*Gaussian Component

Table 5: Same as Table 4 but for PASH Cations

Wavelength ( $\mu\text{m}$ )	FWHM ( $\mu\text{m}$ )	Intensity ( $10^{-25} \text{cm}^3$ per S)
9.95	0.55	6.60
10.87	0.56	1.18
12.40	0.81	3.24
13.81	0.36	0.15
15.35	2.26	1.00
17.55	0.96	0.98
19.45	2.06	2.58
21.35*	1.86	1.18
25.93	1.96	2.63

\*Gaussian Component